Derivative Riemann Solvers for Systems of Conservation Laws and ADER Methods

E. F. Toro

Laboratory of Applied Mathematics
Faculty of Engineering, University of Trento
Trento, Italy
E-mail: toro@ing.unitn.it
Website: http://www.ing.unitn.it/toro

V. A. Titarev

Department of Mathematics
Faculty of Science, University of Trento
Trento, Italy
E-mail: titarev@science.unitn.it
Website: http://www.science.unitn.it/∼titarev

Key words: Hyperbolic systems, derivative Riemann problem, piece-wise smooth data, evolved-data Riemann solvers, arbitrary-order schemes, ADER method.

Abstract

In this paper we first briefly review the semi-analytical method [20] for solving the Derivative Riemann Problem for systems of hyperbolic conservation laws with source terms. Next, we generalize it to hyperbolic systems for which the Riemann problem solution is not available. As an application example we implement the new derivative Riemann solver in the high-order finite-volume ADER advection schemes. We provide numerical examples for the compressible Euler equations in two space dimensions which illustrate robustness and high accuracy of the resulting schemes.

1 Introduction

Conventionally, the Riemann problem for a system of conservation laws is defined as the Cauchy problem with initial conditions consisting of two constant states separated by a discontinuity at the origin. As is well known, the solution of such problem can then be used locally to construct upwind finite volume numerical methods [5]. The required intercell numerical flux is obtained by a time-integral average of the solution of the Riemann problem at the interface of a volume or element. In this manner, the conventional *piece-wise* *constant data* Riemann problem can be associated with a first-order numerical method, a Godunov method [5]. A generalization of this approach results in second-order methods [1, 8], whereby a *piece-wise linear data* Riemann problem is posed and solved. This Riemann problem has become to be known as the Generalized Riemann problem. A further generalization is to consider the Riemann problem for a system of equations with source terms and *arbitrary piece-wise smooth* initial data [20]. In particular, the initial conditions may consist of polynomials of arbitrary degree. Here we call such Riemann problem, the *Derivative Riemann Problem*, or DRP for short. The numerical fluxes resulting from the DRP give rise to the high-order ADER-type schemes, e.g. [18, 14, 13, 10, 22, 15, 4].

The solution procedure for the DRP reported in [20] provides an approximation to the state variable along the t-axis in the form of a Taylor time expansion. To build up this expansion, the original DRP is reduced to a sequence of *conventional* Riemann problems for *homogeneous* advection equations. The leading term of the expansion is computed as the Godunov state of the conventional nonlinear Riemann problem, whereas the evaluation of higher-order terms involves the solution of linearized Riemann problems for spatial derivatives. Therefore, availability of an approximate-state Riemann solver for the non-linear conventional Riemann problem system is crucial for building up the approximate solution to the DRP. Although exact or approximate-state Riemann solvers are available for a large variety of hyperbolic systems of conservation laws [16, 7], for complex nonlinear systems they may become very complicated or simply unavailable. It is therefore desirable to have a simple procedure for calculating the leading term of the state expansion which would not necessarily require a detailed knowledge of the Riemann problem solution.

The aim of the present paper is twofold. Firstly, we present a new method to compute the leading term of the Taylor time expansion which does not require a Riemann solver for the nonlinear system to be solved. This method proceeds first to a non-linear evolution of the initial condition of a conventional Riemann problem, followed by a simple linearization of the Riemann problem, which leads to closed-form solutions. We illustrate the method by solving the DRP for the inviscid Burgers' equation with a source term. Secondly, we incorporate the new variant of the DRP solver into high order finite volume ADER methods for hyperbolic systems. We assess the performance of the resulting schemes for a number of test problems for the Euler equations and compare them with the existing ADER [15] and WENO [11] schemes.

The rest of the paper is organized as follows. In Section 2 we review the current DRP solver. In Section 3 we present a new procedure to compute the leading term and provide a numerical example to illustrate its accuracy. In Section 4 we describe the application to the ADER approach. Numerical examples for the two-dimensional compressible Euler equations are given in Section 5 and conclusions are drawn in Section 6.

2 The Derivative Riemann Problem

2.1 The Problem

The Derivative Riemann Problem or DRP for a hyperbolic system is the initial-value problem

$$\left.\begin{array}{l} \partial_t \mathbf{Q} + \partial_x \mathbf{F}(\mathbf{Q}) = \mathbf{S}(x,t,\mathbf{Q}) \ , \\ \mathbf{Q}(x,0) = \left\{ \begin{array}{lll} \mathbf{Q}_L(x) & \text{if} & x < 0 \ , \\ \mathbf{Q}_R(x) & \text{if} & x > 0 \ . \end{array} \right. \end{array} \right\} \tag{1}$$

where the initial states $\mathbf{Q}_L(x)$, $\mathbf{Q}_R(x)$ are two vectors, the components of which are smooth functions of distance x. We introduce the notation DRP$_K$ to mean the Derivative Riemann Problem in which K represents the number of non-trivial spatial derivatives of the initial condition, $K = \max\{K_L, K_R\}$, where K_L and K_R are such that

$$\partial_x^{(k)} \mathbf{Q}_L(x) \equiv 0 \ \ \forall k > K_L \ , \ \forall x < 0 \ \text{and} \ \partial_x^{(k)} \mathbf{Q}_R(x) \equiv 0 \ \ \forall k > K_R \ , \ \forall x > 0 \ .$$

DRP$_0$ means that all first ($k = 1$) and higher-order spatial derivatives of the initial condition for the DRP away from the origin vanish identically; this case corresponds to the conventional piece-wise constant data Riemann problem.

2.2 Solution Methodology

Recall that the two initial states $\mathbf{Q}_L(x)$ and $\mathbf{Q}_R(x)$ are assumed to be smooth functions, for example $K-$th order polynomials, defined respectively for $x < 0$ and for $x > 0$, with a discontinuity at $x = 0$. Away from $x = 0$ we could use the Cauchy-Kowalewski method to construct a solution $\mathbf{Q}(x,t)$ to (1), provided that all the smoothness assumptions of the Cauchy-Kowalewski theorem were met. Here we are interested in the solution of DRP$_K$, right at $x = 0$, where in fact the initial data may be discontinuous.

Fig. 1 illustrates the initial conditions of the DRP$_K$ and the information available at $t = 0$ at the origin $x = 0$. The initial data is, in general, discontinuous at $x = 0$. Away from $x = 0$ the initial data is smooth, with all spatial derivatives well defined and readily computed. At $x = 0$ we can define one-sided spatial derivatives, so that at the interface $x = 0$ we have jumps in spatial derivatives. These jumps will form the initial data for new (conventional) Riemann problems, as we shall explain below.

We seek a power series solution at $x = 0$ as a function $\mathbf{Q}_{LR}(t)$ of time t only. Formally, we write the sought solution as

$$\mathbf{Q}_{LR}(\tau) = \mathbf{Q}(0, 0_+) + \sum_{k=1}^{K} \left[\partial_t^{(k)} \mathbf{Q}(0, 0_+) \right] \frac{\tau^k}{k!} \ , \tag{2}$$

where $0_+ \equiv \lim\limits_{t \to 0_+} t$. The solution contains a leading term $\mathbf{Q}(0, 0_+)$ and higher-order

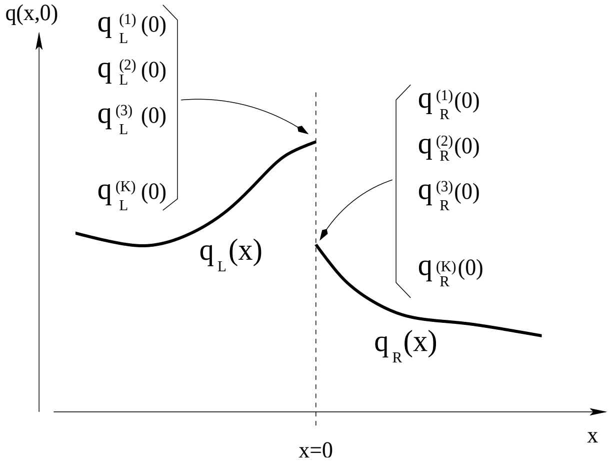

Figure 1: Information available in the $\mathbf{DRP}_K$ for a scalar problem. The data states $q_L(x)$ and $q_R(x)$ are smooth functions away from $x = 0$ and have one-sided spatial derivatives at $x = 0$.

terms with coefficients determined by $\partial_t^{(k)}\mathbf{Q}(0, 0_+)$. In what follows we describe a method to compute each of the terms of the series expansion.

2.2.1 The leading term

The leading term $\mathbf{Q}(0, 0_+)$ in the expansion accounts for the *first-instant* interaction of the initial data via the governing PDEs, which is realized solely by the boundary extrapolated values $\mathbf{Q}_L(0)$ and $\mathbf{Q}_R(0)$ in (1). Therefore, the leading term $\mathbf{Q}(0, 0_+)$ is found from the *similarity solution* of the following $\mathbf{DRP}_0$

$$\left.\begin{array}{l} \partial_t\mathbf{Q} + \partial_x\mathbf{F}(\mathbf{Q}) = \mathbf{0} \ , \\ \mathbf{Q}(x,0) = \left\{ \begin{array}{lll} \mathbf{Q}_L(0) \equiv \lim_{x\to 0_-} \mathbf{Q}_L(x) & \text{if} & x < 0 \ , \\ \mathbf{Q}_R(0) \equiv \lim_{x\to 0_+} \mathbf{Q}_R(x) & \text{if} & x > 0 \ . \end{array}\right. \end{array}\right\} \tag{3}$$

Here, the influence of the source term can be neglected. Denoting the similarity solution by $\mathbf{D}^{(0)}(x/t)$, the sought leading term is given by evaluating this solution along the t-axis, that is along $x/t = 0$, namely

$$\mathbf{Q}(0, 0_+) = \mathbf{D}^{(0)}(0) \ . \tag{4}$$

The value $\mathbf{D}^{(0)}(0)$ is commonly known as the *Godunov state*, as it corresponds to the numerical flux associated with the first-order upwind scheme of Godunov [5]. In what follows we shall extend the use of this terminology to mean the solution of conventional Riemann problems for spatial derivatives evaluated at $x/t = 0$. In practice, a conventional *Riemann solver*, possibly approximate, is needed here to determine the leading term.

2.2.2 Higher-order terms

To compute the higher-order terms in (2) we need to compute the coefficients, that is the partial derivatives $\partial_t^{(k)}\mathbf{Q}(x,t)$ at $x = 0$, $t = 0_+$. If these were available on both sides of the initial discontinuity at $x = 0$, then one could implement a fairly direct approach to the evaluation of the higher order terms. The method presented below relies on the availability of all spatial derivatives rather than temporal derivatives away from the interface, see Fig. 1.

In order to express all *time* derivatives as *functions of space derivatives* we apply the Cauchy-Kowalewski method and use the fact that both the physical flux and source term are the functions of the vector of conservative variables. This yields the following expressions for time derivatives:

$$\partial_t^{(k)}\mathbf{Q}(x,t) = \mathbf{P}^{(k)}(\partial_x^{(0)}\mathbf{Q}, \partial_x^{(1)}\mathbf{Q}, \ldots, \partial_x^{(k)}\mathbf{Q}) \ . \tag{5}$$

These time-partial detivatives at $x = 0$ for $t > 0$ have a meaning if the spatial derivatives $\partial_x^{(0)}\mathbf{Q}, \partial_x^{(1)}\mathbf{Q}, \ldots, \partial_x^{(k)}\mathbf{Q}$ can be given a meaning at $x = 0$ for $t > 0$. For $x < 0$ and for $x > 0$ all spatial derivatives

$$\partial_x^{(k)}\mathbf{Q}_L(x) \ , \ \ \partial_x^{(k)}\mathbf{Q}_R(x) \ , \ \ k = 1, 2, \ldots, K$$

are defined and readily computed. At $x = 0$, however, we have the *one-sided* derivatives

$$\left.\begin{array}{l} \partial_x^{(k)}\mathbf{Q}_L(0) = \lim_{x\to 0_-} \partial_x^{(k)}\mathbf{Q}_L(x) \\ \\ \partial_x^{(k)}\mathbf{Q}_R(0) = \lim_{x\to 0_+} \partial_x^{(k)}\mathbf{Q}_R(x) \end{array}\right\} \ k = 1, 2, \ldots, K \ .$$

See Fig. 1. We thus have a set of K pairs $(\partial_x^{(k)}\mathbf{Q}_L(0), \partial_x^{(k)}\mathbf{Q}_R(0))$ of constant vectors that could be used as the initial condition for K conventional Riemann problems, if in addition we had a set of corresponding evolution equations for the quantities $\partial_x^{(k)}\mathbf{Q}(x,t)$. The sought evolution equations can be easily constructed. It can be verified that the quantity $\partial_x^{(k)}\mathbf{Q}(x,t)$ obeys the following system of non-linear inhomogeneous evolution equations

$$\partial_t(\partial_x^{(k)}\mathbf{Q}(x,t)) + \mathbf{A}(\mathbf{Q})\partial_x(\partial_x^{(k)}\mathbf{Q}(x,t)) = \mathbf{H}^k \ . \tag{6}$$

where the coefficient matrix $\mathbf{A}(\mathbf{Q})$ is precisely the Jacobian matrix of system (1). Equations (6) are obtained by manipulating derivatives of (1). The source term $\mathbf{H}^k$ on the right hand side of (6)

$$\mathbf{H}^k = \mathbf{H}^k(\partial_x^{(0)}\mathbf{Q}(x,t), \partial_x^{(1)}\mathbf{Q}(x,t), \ldots, \partial_x^{(k)}\mathbf{Q}(x,t))$$

is a function of the spatial derivatives $\partial_x^{(k)}\mathbf{Q}(x,t)$, for $k = 0, 1, \ldots, k$, and vanishes when the Jacobian matrix $\mathbf{A}$ is constant and $\mathbf{S} \equiv 0$, that is, when the original system in (1) is linear and homogeneous with constant coefficients. In order to easily solve these evolution equations we perform two simplifications, namely, we first neglect the source terms $\mathbf{H}^k$ and then we linearize the resulting homogeneous equations.

Neglecting the effect of the source terms $\mathbf{H}^k$ is justified, as we only need $\partial_x^{(k)}\mathbf{Q}(x,t)$ at the *first-instant* interaction of left and right states. We thus have homogeneous nonlinear systems for spatial derivatives. Then we perform a linearization of the homogeneous systems about the leading term of the power series expansion (2), that is the coefficient matrix is taken as the constant matrix

$$\mathbf{A}_{LR}^{(0)} = \mathbf{A}(\mathbf{Q}(0,0_+)) \ .$$

Thus, in order to find the spatial derivatives at $x = 0$, $t = 0_+$ we solve the following *homogeneous, linearized* conventional Riemann problems

$$\left.\begin{array}{l} \partial_t(\partial_x^{(k)}\mathbf{Q}(x,t)) + \mathbf{A}_{LR}^{(0)}\partial_x(\partial_x^{(k)}\mathbf{Q}(x,t)) = \mathbf{0} \ , \\ \partial_x^{(k)}\mathbf{Q}(x,0) = \left\{ \begin{array}{ll} \partial_x^{(k)}\mathbf{Q}_L(0) \ , & x < 0 \ , \\ \partial_x^{(k)}\mathbf{Q}_R(0) \ , & x > 0 \ . \end{array} \right. \end{array} \right\} \tag{7}$$

Note that the (constant) Jacobian matrix $\mathbf{A}_{LR}^{(0)}$ is the same coefficient matrix for all $\partial_x^{(k)}\mathbf{Q}(x,t))$ and is evaluated only once, using the leading term of the expansion.

We denote the similarity solution of (7) by $\mathbf{D}^{(k)}(x/t)$. In the computation of all higher order terms, the solutions of the associated Riemann problems are analytic and the question of choosing a *Riemann solver* does not arise. The relevant value at the interface is obtained by evaluating this vector at $x/t = 0$, namely

$$\partial_x^{(k)}\mathbf{Q}(0,0_+)) = \mathbf{D}^{(k)}(0) \ .$$

We call this value the *Godunov state*, in analogy to the interface state (4) associated with the leading term.

Having evolved all space derivatives at the interface $x = 0$ we form the time derivatives and finally define the solution of the $\mathbf{DRP}_K$ as the power series expansion

$$\mathbf{Q}_{LR}(\tau) = \mathbf{C_0} + \mathbf{C_1}\tau + \mathbf{C_2}\tau^2 + \ldots + \mathbf{C_K}\tau^K \ . \tag{8}$$

where the coefficients are given by

$$\mathbf{C}_k = \frac{\partial_t^{(k)}\mathbf{Q}(0,0_+))}{k!} \ . \tag{9}$$

2.2.3 Summary of the method

The solution of the Derivative Riemann Problem has the following steps:

- **Step (I): The leading term**

  To compute the leading term one solves exactly or approximately the conventional Riemann problem (3) to obtain the similariry solution $\mathbf{D}^{(0)}(x/t)$. The leading term in then given by the Godunov state $\mathbf{Q}(0, 0_+)) = \mathbf{D}^{(0)}(0)$.

- **Step (II): Higher order terms**

  1. **Time derivatives in terms of spatial derivatives**

     Use the Cauchy-Kowalewski method to express time derivatives $\partial_t^{(k)}\mathbf{Q}(x,t)$ in terms of functions of space derivatives as in (5)

  2. **Evolution equations for derivatives**

     Construct evolution equations for spatial derivatives (6).

  3. **Riemann problems for spatial derivatives**

     Simplify (6) by neglecting source terms and linearizing the evolution equations. Then pose conventional, homogeneous linearized Riemann problems for spatial derivatives (7).

     Solve analytically these Riemann problems to obtain similarity solutions $\mathbf{D}^{(k)}(x/\tau)$ and set $\partial_x^{(k)}\mathbf{Q}(0, 0_+)) = \mathbf{D}^{(k)}(0)$.

- **Step (III):** Form the solution as the power series expansion (8) with the coefficients (9).

3 Riemann Solvers for the Leading Term of DRP

Recall that the leading term of the Taylor series expansion (2), the Godunov state, will be the solution of a non-linear problem, found by a non-linear Riemann solver, exact or approximate. As has already been mentioned, for complex nonlinear systems such solvers are very complicated or simply unavailable. It is therefore desirable from the practical point of view to have a simple procedure for calculating the leading term of the state expansion which would not require a detailed knowledge of the Riemann problem solution.

3.1 EVILIN Riemann Solver

Here, we suggest that the recently-proposed EVILIN Riemann solver [17] be used to obtain the Godunov state of the nonlinear Riemann problem (2). The computation of the Godunov state by the EVILIN Riemann solver consists of two main steps. The first step is to open the Riemann fan by using the generalized **M**ulti-**S**tage (GMUSTA) Riemann solver [21]. The GMUSTA Riemann solver solves the local Riemann problem

(3) numerically rather than analytically by means of a simple first-order scheme applying transmissive boundary conditions at each local time step. This is equivalent to evolving in time the initial data $\mathbf{Q}_L(0)$, $\mathbf{Q}_R(0)$ via the governing equations. In the second step one applies a linearized Riemann solver on the *evolved* initial data obtained from the GMUSTA procedure giving a close-form expression for the Godunov state.

Below we briefly outline the GMUSTA and EVILIN Riemann solvers. Assume that at initial time $t = 0$ we know the left and right initial data values $\mathbf{Q}_L(0)$, $\mathbf{Q}_R(0)$ of the Riemann problem (3). We introduce a local spatial domain and the corresponding mesh with $2M$ cells: $-M + 1 \leq m \leq M$ and cell size Δx. The boundary between cells $m = 0$ and $m = 1$ corresponds to the interface position $x = 0$ in (3). Transmissive boundary conditions are applied at numerical boundaries $x_{\pm M+1/2}$ on the grounds that the Riemann - like data extends to $\pm\infty$. We now want to solve this Riemann problem numerically on a given local mesh and construct a sequence of *evolved* data states $\mathbf{Q}_m^{(l)}$, $0 \leq l \leq k$ in such a way, that the final values adjacent to the origin $\mathbf{Q}_0^{(k)}$, $\mathbf{Q}_1^{(k)}$ are close to the sought Godunov state. Here k is the total number of local time steps, or stages of the algorithm.

In short, the GMUSTA local time marching for $m = -M + 1, \ldots M$ is organized as follows:

$$\mathbf{Q}_m^{(l+1)} = \mathbf{Q}_m^{(l)} - \frac{\Delta t_{loc}}{\Delta x}\left(\mathbf{F}_{m+1/2}^{(l)} - \mathbf{F}_{m-1/2}^{(l)}\right), \quad \mathbf{F}_{m+1/2}^{(l)} = \mathbf{F}^{GF}(\mathbf{Q}_m^{(l)}, \mathbf{Q}_{m+1}^{(l)}). \tag{10}$$

Here $\mathbf{F}^{GF}$ is the monotone first order GFORCE numerical flux [21] which is the upwind generalization of the centred FORCE flux [16] and is given by:

$$\mathbf{F}^{GF} = \Omega_{loc}\mathbf{F}^{LW} + (1 - \Omega_{loc})\mathbf{F}^{LF}, \quad \Omega_{loc} = \frac{1}{1 + C_{loc}}, \tag{11}$$

where $\mathbf{F}^{LW}$ and $\mathbf{F}^{LF}$ are the centred Lax-Wendroff and Lax-Friedrichs fluxes, respectively. The local time step Δt_{loc} is computed from the local Courant number coefficient $0 < C_{loc} < 1$ and then is used in the time update and for evaluation $\mathbf{F}^{LW}$ and $\mathbf{F}^{LF}$.

We remark that although expression (11) involves centred fluxes, the resulting GFORCE flux is upwind due to the the fact that the nonlinear weight Ω_{loc} in (11) depends on the local wave speed. We remark that in the special case of the linear constant coefficient equation the GFORCE flux is identical to the Godunov upwind flux.

The time marching procedure is stopped when the desired number of stages k is reached. At the final stage we have a pair of values adjacent to the interface position. For the construction of Godunov-type advection schemes one needs a numerical flux at the origin, which for the outlined procedure is given by

$$\mathbf{F}_{i+1/2}^{GM} = \mathbf{F}_{m+1/2}^{(k)} = \mathbf{F}^{GF}(\mathbf{Q}_m^{(k)}, \mathbf{Q}_{m+1}^{(k)}). \tag{12}$$

For the purpose of solving the derivative Riemann problem, however, we need the Godunov state as well. In general, the states adjacent to the origin, namely $\mathbf{Q}_0^{(k)}$,$\mathbf{Q}_1^{(k)}$ are different.

We now use a linearized Riemann solver to resolve the discontinuity in $\mathbf{Q}$ at the origin resulting in the EVILIN Riemann solver [17]. To this end we solve exactly the following linearized Riemann problem:

$$
\begin{aligned}
&\partial_t \mathbf{Q} + \mathbf{A}_{1/2}\partial_x \mathbf{Q} = \mathbf{0}, \quad \mathbf{A}_{1/2} = \mathbf{A}(\tfrac{1}{2}(\mathbf{Q}_0^{(k)} + \mathbf{Q}_1^{(k)})) \\
&\mathbf{Q}(x,0) = \begin{cases} \mathbf{Q}_0^{(k))} & \text{if} \quad x < 0 \ , \\ \mathbf{Q}_1^{(k))} & \text{if} \quad x > 0 \ . \end{cases}
\end{aligned}
\tag{13}
$$

We remark that conventional linearized Riemann solvers have two major deficiencies. Firstly, they give a large unphysical jump in all flow variables near sonic points, a *rarefaction shock*, unless explicit *entropy fixes* are enforced. This is due to the fact that linearized Riemann solvers do not open the Riemann fan when the solution contains a sonic point and produce instead a rarefaction shock. Secondly, they cannot handle the situation when the Riemann problem solution contains very strong rarefaction waves. These problems do not occur for the EVILIN Riemann solver, which is essentially due to the fact that we apply the linearized Riemann solver to *evolved* values rather than to the initial data. See [17] for more details and numerical examples.

It can be shown numerically [21] that when the number of cells $2M$ and number of stages k are large, the GMUSTA flux converges to the Godunov flux with the exact Riemann solver. Correspondingly, the approximate Godunov state produced by the EVILIN solver (13) converges to the exact Godunov state, even for nonlinear systems with a complex wave pattern. For the linear constant coefficient equations this property is exact, whereas for nonlinear systems it can be verified by numerical experiments.

We note that since the solution of the piece-wise constant Riemann problem (3) is self-similar, the value of the cell size Δx used in the local time marching does not influence the resulting GMUSTA and EVILIN solutions. For a given CFL number C_{loc} these solutions depend only on the number of stages k and domain size $2M$. Moreover, when $M > k$ the transmissive boundary conditions do not affect the numerical solution of (3) which in this case depends only on k and C_{loc}.

3.2 Numerical example

As an example here we solve the following derivative Riemann problem for the inviscid inhomogeneous Burgers' equation:

$$
\left.
\begin{aligned}
&\partial_t q + \partial_x(\tfrac{1}{2}q^2) = e^{-q} \\
&q(x,0) = \begin{cases} q_L(x) = e^{-2(x-\frac{1}{5})^2} & \text{if} \quad x < 0 \\ \\ q_R(x) = \frac{1}{4}e^{-2(x+\frac{1}{5})^2} & \text{if} \quad x > 0 \end{cases}
\end{aligned}
\right\}
\tag{14}
$$

Fig. 2 shows the *global* solution of (14) in the $x - t$ plane. This solution was obtained

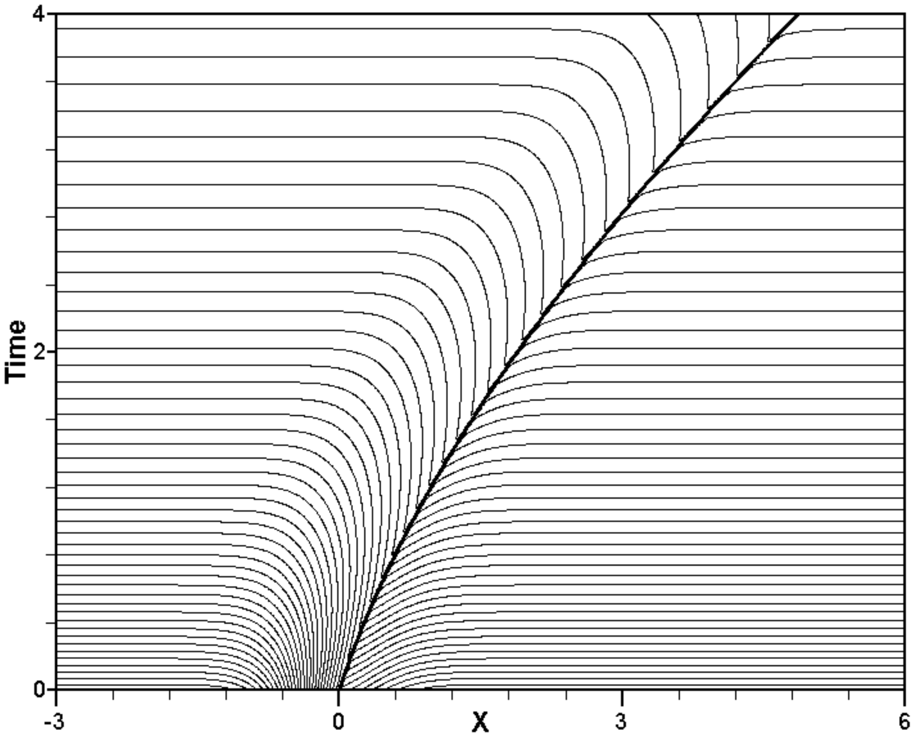

Figure 2: Numerical solution of DRP problem (14)

numerically using a high-order non-oscillatory numerical method on a very fine mesh. The dominant feature of the solution is an accelerating shock wave that emerges from the initial discontinuity in the initial condition at $x = 0$. We regard this as the exact solution and define an error by taking the difference between the accurate numerical solution and our semi-analytical DRP solution (2).

Table 1 shows the variation of the error as function of the order of accuracy of the Taylor time expansion for different times τ using the exact Riemann solver for the leading term of the time expansion. As expected, for sufficiently small output times the error rapidly decreases when the number of terms in the expansion increases. For the last output time $\tau = 0.2$ the solution appears to be too far away from the initial time and therefore the Taylor time expansion (2) is not accurate anymore.

Tables 2–3 show the convergence study for the case when the EVILIN Riemann solver is used for the leading term of the time expansion. These tables illustrate the influence of the number of cells $2M$ and stages k in the local time marching (10) on the accuracy of the resulting Taylor time expansion (2). As expected, the size of the error is defined by the accuracy of the leading term. That is the error committed in computing the leading term of the state expansion (2) by using the EVILIN approximation (13) cannot be recovered by high order terms. From the tables it is clear that this error crucially depends on the number of stages k and cells $2M$ in the GMUSTA time marching (10). As M and k grow, the leading term obtained by EVILIN approximation approaches the exact one and the

EVILIN solution converges to the one obtained by using the exact Riemann solver, see Table 3.

4 Use of the DRP in the ADER approach

The DRP Riemann solver described in the previous sections can be used to construct very high-order numerical ADER-type fluxes to be used in ADER and ADER-DG schemes. For simplicity, in this section we review the use of the DRP solver for the construction of ADER schemes as applied to the one-dimensional homogeneous systems only [14]. Extension to multiple space dimensions and source terms is straightforward and can be found in [22, 15].

Consider a hyperbolic system in conservation form given by

$$\partial_t \mathbf{Q} + \partial_x \mathbf{F}(\mathbf{Q}) = \mathbf{0} \tag{15}$$

along with initial and boundary conditions. Here $\mathbf{Q}$ is the vector of unknown conservative variables and $\mathbf{F}(\mathbf{Q})$ is the physical flux vector. Integrating (15) over a space-time control volume in $x - t$ space $[x_{i-1/2}, x_{i+1/2}] \times [t^n, t^{n+1}]$ of dimensions $\Delta x = x_{i+1/2} - x_{i-1/2}$, $\Delta t = t^{n+1} - t^n$, we obtain the following one-step finite-volume scheme:

$$\mathbf{Q}_i^{n+1} = \mathbf{Q}_i^n + \frac{\Delta t}{\Delta x}\left(\mathbf{F}_{i-1/2} - \mathbf{F}_{i+1/2}\right). \tag{16}$$

Here $\mathbf{Q}_i^n$ is the cell average of the solution at time level t^n and $\mathbf{F}_{i+1/2}$ is the time average of the physical flux at cell interface $x_{i+1/2}$ term:

$$\mathbf{Q}_i^n = \frac{1}{\Delta x}\int\limits_{x_{i-1/2}}^{x_{i+1/2}} \mathbf{Q}(x, t^n)\, dx, \quad \mathbf{F}_{i+1/2} = \frac{1}{\Delta t}\int\limits_{t^n}^{t^{n+1}} \mathbf{F}(\mathbf{Q}(x_{i+1/2}, t))\, dt. \tag{17}$$

The first step in the ADER algorithm is the reconstruction of point-wise values of the solution from cell averages at $t = t^n$ via high-order polynomials. To circumvent the Godunov theorem [5] and design non-oscillatory schemes we use the nonlinear (solution-adaptive) weighted essentially non-oscillatory (WENO) reconstruction, see [2, 11] and references therein. After the reconstruction step the conservative variables in each cell are represented by vectors $\mathbf{p_i}(x)$ of polynomials. Then at each cell interface we can pose the following derivative Riemann problem:

$$\begin{aligned} &\partial_t \mathbf{Q} + \partial_x \mathbf{F}(\mathbf{Q}) = \mathbf{0}, \\ &\mathbf{Q}(x, 0) = \begin{cases} \mathbf{Q}_L(x) = \mathbf{p}_i(x), & x < x_{i+1/2}, \\ \mathbf{Q}_R(x) = \mathbf{p}_{i+1}(x), & x > x_{i+1/2}. \end{cases} \end{aligned} \tag{18}$$

Obviously, the initial-boundary problem (18) is exactly the Derivatie Riemann problem (1). Therefore, in order to obtain an approximate solution for the interface state

Table 1: Convergence study for the Derivative Riemann problem (14) for different output times τ and different orders of accuracy. The exact Riemann solver is used.

Order	$t = 0.01$	$t = 0.05$	$t = 0.1$	$t = 0.2$
1	0.2918×10^{-2}	0.1573×10^{-1}	0.1573×10^{-1}	0.6580×10^{-1}
2	0.7381×10^{-4}	0.1513×10^{-2}	0.1512×10^{-2}	0.8916×10^{-2}
3	0.3479×10^{-5}	0.4197×10^{-3}	0.4197×10^{-3}	0.2200×10^{-1}
4	0.2452×10^{-7}	0.1830×10^{-4}	0.1830×10^{-4}	0.6032×10^{-2}
5	0.1389×10^{-8}	0.3843×10^{-5}	0.3843×10^{-5}	0.2331×10^{-2}
6	0.3771×10^{-10}	0.6143×10^{-6}	0.6143×10^{-6}	0.2234×10^{-2}

Table 2: Convergence study for the Derivative Riemann problem (14) for different output times τ and different orders of accuracy. The EVILIN Riemann solver with $M = 1$ and $k = 2$ is used for the leading term.

Order	$t = 0.01$	$t = 0.05$	$t = 0.1$	$t = 0.2$
1	0.3097×10^{-2}	0.9719×10^{-2}	0.2699×10^{-1}	0.5979×10^{-1}
2	0.5873×10^{-2}	0.4161×10^{-2}	0.7710×10^{-3}	0.4269×10^{-2}
3	0.5949×10^{-2}	0.6063×10^{-2}	0.8381×10^{-2}	0.2617×10^{-1}
4	0.5946×10^{-2}	0.5633×10^{-2}	0.4936×10^{-2}	0.1385×10^{-2}
5	0.5947×10^{-2}	0.5647×10^{-2}	0.5165×10^{-2}	0.2269×10^{-2}
6	0.5946×10^{-2}	0.5651×10^{-2}	0.5303×10^{-2}	0.6708×10^{-2}

Table 3: Convergence study for the Derivative Riemann problem (14) for different output times τ and different order of accuracy. The EVILIN Riemann solver with $M = 3$ and $k = 12$ is used for the leading term.

Order	$t = 0.01$	$t = 0.05$	$t = 0.1$	$t = 0.2$
1	0.2918×10^{-2}	0.1573×10^{-1}	0.3300×10^{-1}	0.6580×10^{-1}
2	0.7381×10^{-4}	0.1512×10^{-2}	0.4560×10^{-2}	0.8916×10^{-2}
3	0.3479×10^{-5}	0.4197×10^{-3}	0.3168×10^{-2}	0.2200×10^{-1}
4	0.2452×10^{-7}	0.1830×10^{-4}	0.3356×10^{-3}	0.6032×10^{-2}
5	0.1389×10^{-8}	0.3843×10^{-5}	0.1042×10^{-3}	0.2331×10^{-2}
6	0.3783×10^{-10}	0.6143×10^{-6}	0.3840×10^{-4}	0.2234×10^{-2}

$\mathbf{Q}(x_{i+1/2}, \tau)$, where τ is local time $\tau = t - t^n$, we apply the solution procedure outlined above and obtain the solution in the form of the temporal polynomial (2).

Two options now exist to evaluate the numerical flux depending on the way we evaluate the Godunov state of (3). If a conventional approximate-state Riemann solver for the Riemann problem (3) is available we use the *state-expansion* ADER [14]. We insert the approximate state $\mathbf{Q}(\tau))$ into the definition of the numerical flux (17) and then use an appropriate r^{th}-order accurate quadrature for time integration:

$$\mathbf{F}_{i+1/2} = \sum_{l=0}^{K_l} \mathbf{F}(\mathbf{Q}(x_{i+1/2}, \alpha_l \Delta t))\omega_l. \tag{19}$$

Here α_l and ω_l are properly scaled nodes and weights of the rule and K_l is the number of nodes.

When a conventional approximate-state Riemann solver is not available, we use the EVILIN Riemann solver to obtain the leading term of the state expansion (2). Numerical experiments show that in this case the best results are obtained when the so-called *flux-expansion* ADER [15] is used. The main difference from the state-expansion ADER is that we now seek a truncated Taylor time expansion of the physical flux at $x_{i+1/2}$:

$$\mathbf{F}(x_{i+1/2}, \tau) = \mathbf{F}(x_{i+1/2}, 0+) + \sum_{k=1}^{r-1} \left[\frac{\partial^k}{\partial t^k} \mathbf{F}(x_{i+1/2}, 0+) \right] \frac{\tau^k}{k!}. \tag{20}$$

From (17) and (20) the numerical flux is now given by

$$\mathbf{F}_{i+1/2} = \mathbf{F}(x_{i+1/2}, 0+) + \sum_{k=1}^{r-1} \left[\frac{\partial^k}{\partial t^k} \mathbf{F}(x_{i+1/2}, 0+) \right] \frac{\Delta t^k}{(k+1)!} . \tag{21}$$

The leading term $\mathbf{F}(x_{i+1/2}, 0+)$ accounts for the first interaction of left and right boundary extrapolated values and is the GMUSTA flux (12). Other options include the use of conventional upwind fluxes, see [15] for details. The remaining higher order time derivatives of the flux in (21) are expressed via time derivatives of the intercell state $\mathbf{Q}(x_{i+1/2}, 0+)$, which are known from (1). The leading term $\mathbf{Q}(0+, 0)$ is now given by the EVILIN Riemann solver (13). No numerical quadrature is then required to compute the numerical flux.

An important issue is the choice of parameters M and k in the local GMUSTA time marching (10). In general, we observe that convergence of the EVILIN state to the exact Godunov state is obtained only when $M, k \to \infty$. However, practical experience suggest that for designing *numerical methods* in most of the cases the choice $M = 1$ and $k = 2$ in the GMUSTA time marching (10) gives numerical results that are comparable with those from the most accurate of fluxes, namely, the first-order Godunov upwind flux used in conjunction with the exact Riemann solver. See [21] for a more detailed discussion of the choice of M and k. Therefore, for the rest of the paper we use these values in ADER schemes.

The solution is advanced in time by updating the cell averages according to the one-step formula (16).

5 Application to the Euler Equations

In this section we show some results of the ADER schemes with the new EVILIN-based variant of the DRP solver. We denote the corresponding schemes as ADER-GM schemes. We compare the performance of the new ADER-GM schemes with that of the existing state-expansion ADER-AD schemes from [15] and the state-of-the art finite-volume WENO schemes [11]. For brevity, we consider only schemes with piece-wise parabolic ($r = 3$) polynomials. The resulting schemes (ADER-AD, ADER-GM, WENO) are of fifth order spatial accuracy and third order temporal accuracy. Since the reconstruction step is essentially the same for all methods, the difference in accuracy can result only from the temporal discretization and the numerical fluxes. The ADER schemes use the DRP solver to obtain the numerical flux, whereas the WENO scheme uses the Rusanov-type numerical flux [9] as the building block and third-order TVD RK method [12] for the temporal update.

In all numerical examples we solve the two-dimensional compressible Euler equations of the form

$$\frac{\partial}{\partial t}\mathbf{Q} + \frac{\partial}{\partial x}\mathbf{F}(\mathbf{Q}) + \frac{\partial}{\partial y}\mathbf{G}(\mathbf{Q}) = \mathbf{0}$$

with

$$\mathbf{Q} = \begin{pmatrix} \rho \\ \rho u \\ \rho v \\ E \end{pmatrix}, \quad \mathbf{F} = \mathbf{Q}u + \begin{pmatrix} 0 \\ p \\ 0 \\ pu \end{pmatrix}, \quad \mathbf{G} = \mathbf{Q}v + \begin{pmatrix} 0 \\ 0 \\ p \\ pv \end{pmatrix} \tag{22}$$

$$p = (\gamma - 1)(E - \frac{1}{2}\rho(u^2 + v^2)).$$

Here ρ, u, v, p and E are density, components of velocity in the x and y coordinate directions, pressure and total energy, respectively; γ is the ratio of specific heats. We use $\gamma = 1.4$ throughout.

5.1 Two-dimensional vortex evolution problem

We solve the two-dimensional Euler equations in the square domain $[-5 : 5] \times [-5 : 5]$ with periodic boundary conditions. The initial condition corresponds to a smooth vortex placed at the origin and is defined as the following isentropic perturbation to the uniform flow of unit values of primitive variables [11]:

$$\begin{aligned} u &= 1 - \frac{\varepsilon}{2\pi} e^{\frac{1}{2}(1-r^2)} y, \quad v = 1 + \frac{\varepsilon}{2\pi} e^{\frac{1}{2}(1-r^2)} x, \\ T &= 1 - \frac{(\gamma-1)\varepsilon^2}{8\gamma\pi^2} e^{(1-r^2)}, \quad \frac{p}{\rho^\gamma} = 1, \end{aligned} \tag{23}$$

where $r^2 = x^2 + y^2$ and the vortex strength is $\varepsilon = 5$. The exact solution is a vortex movement with a constant velocity at 45^o to the Cartesian mesh lines. We compute the numerical solution at the output time $t = 20$ for which the vortex returns to the initial position. We use $C_{cfl} = 0.45$ for all runs.

Table 4: Density convergence study for the vortex evolution problem (23) at the output time $t = 20$. $C_{cfl} = 0.45$ is used for all schemes.

Method	Mesh	L_∞ error	L_∞ order	L_1 error	L_1 order
ADER3-AD [15]	25×25	9.71×10^{-2}		5.92×10^{-1}	
	50×50	1.30×10^{-2}	2.90	3.94×10^{-2}	3.91
	100×100	4.14×10^{-4}	4.97	1.54×10^{-3}	4.68
	200×200	9.77×10^{-6}	5.41	5.23×10^{-5}	4.88
ADER3-GM,	25×25	1.01×10^{-1}		6.29×10^{-1}	
present paper	50×50	1.42×10^{-2}	2.83	4.20×10^{-2}	3.91
	100×100	4.58×10^{-4}	4.96	1.63×10^{-3}	4.69
	200×200	9.97×10^{-6}	5.52	5.15×10^{-5}	4.98
WENO [11]	25×25	1.78×10^{-1}		1.12	
	50×50	2.05×10^{-2}	3.11	8.17×10^{-2}	3.78
	100×100	7.01×10^{-4}	4.87	4.44×10^{-3}	4.20
	200×200	3.17×10^{-5}	4.47	1.78×10^{-4}	4.64

Table 4 shows the convergence study for all schemes. We present errors and convergence rates in L_∞ and L_1 norms for cell averages of density. Firstly, we observe that both ADER schemes achieve approximately fifth order of accuracy. The new ADER-GM scheme is only slightly less accurate than the ADER-AD scheme. Secondly, we see that both ADER schemes are more accurate than the WENO scheme by a factor between two and three. The observed difference in accuracy between ADER and WENO schemes can be related to the more accurate time evolution method of the ADER approach as compared to the combination of the Rusanov flux and the TVD RK method in the WENO scheme.

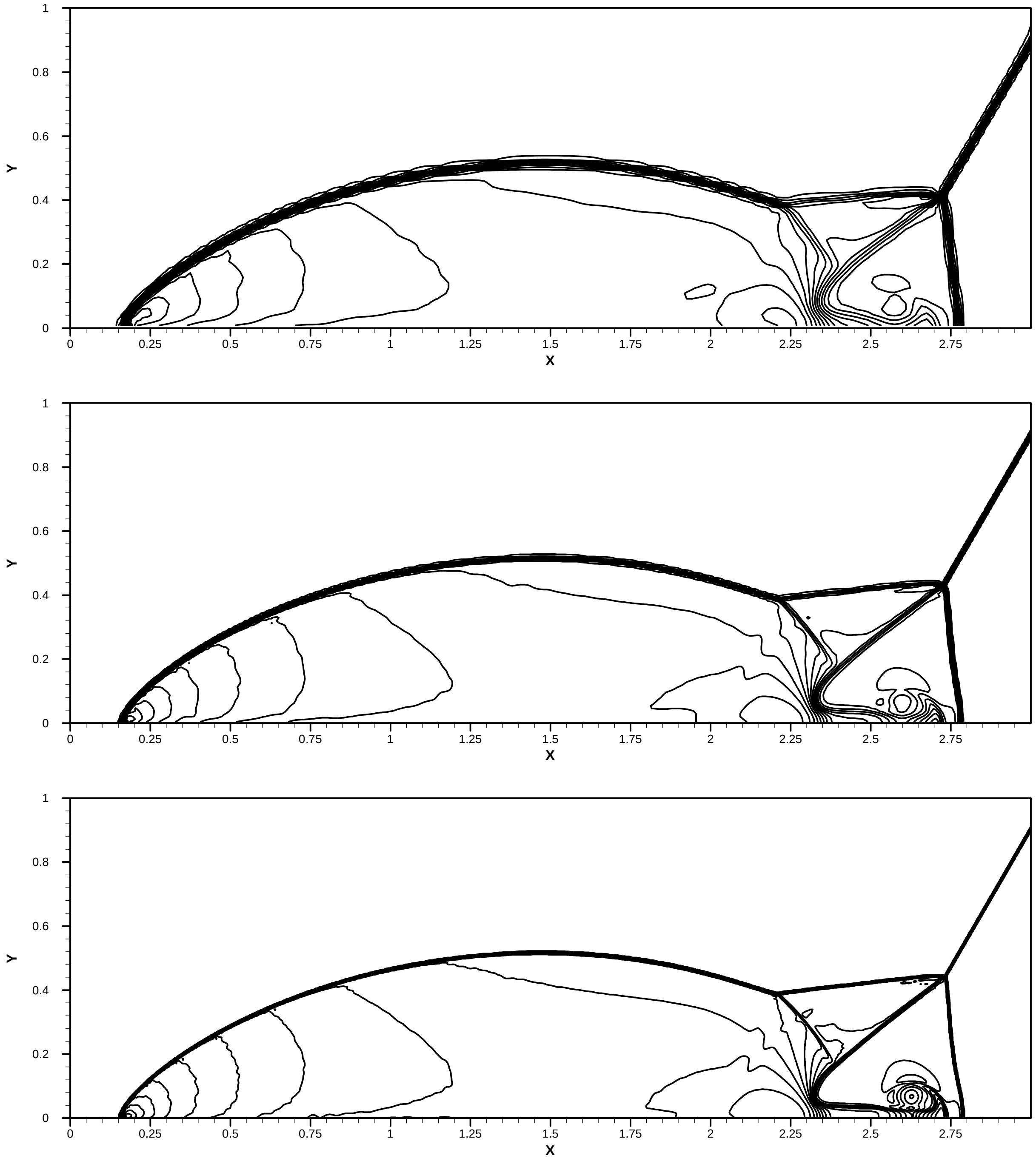

Figure 3: Density convergence study for the double Mach reflection problem. Meshes: 240 × 60 cells (top) , 480 × 120 cells (middle) and 960 × 240 cells (bottom). 30 contour lines from 2 to 22.

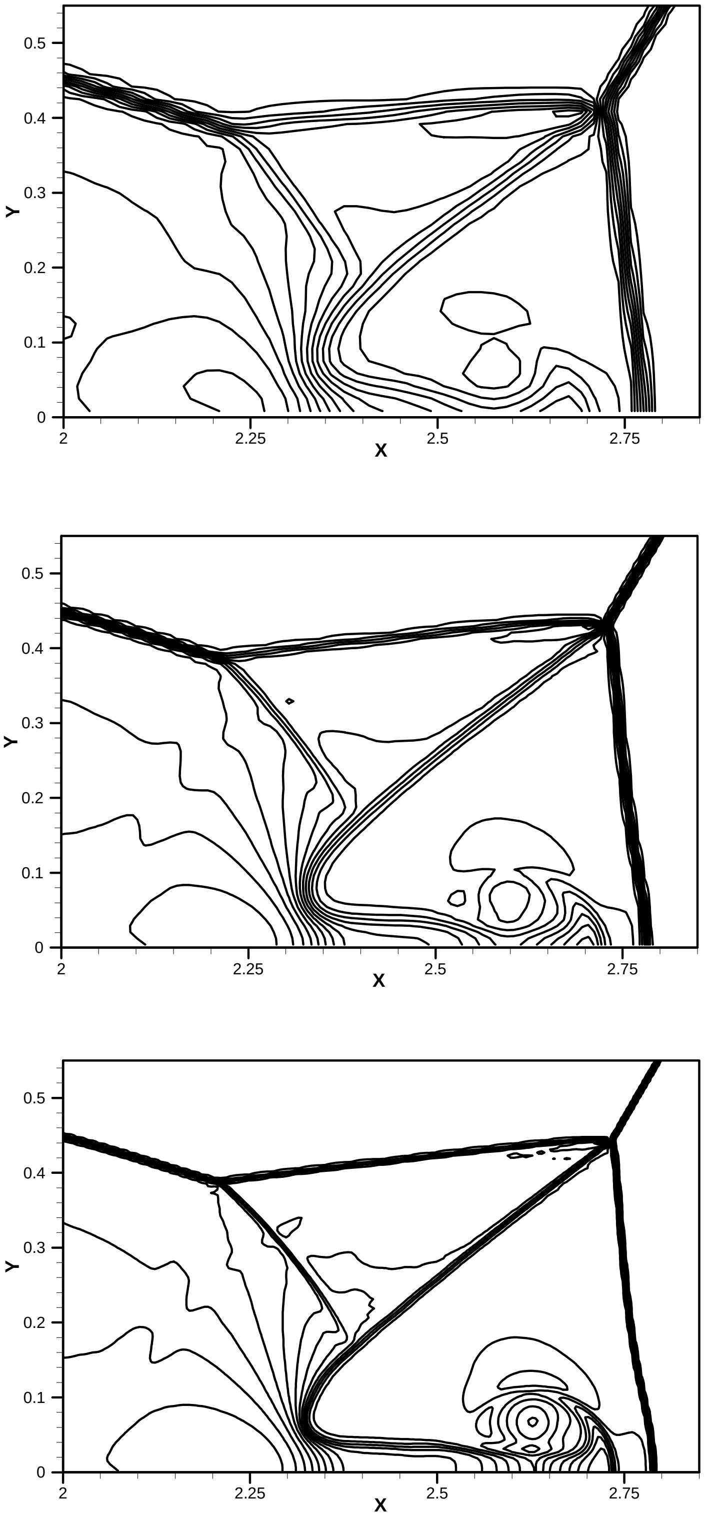

Figure 4: Density convergence study for the double Mach reflection problem. Zoomed area of Fig. 3

5.2 Double Mach reflection of a strong shock

The double Mach reflection problem [23] is a standard test problem for testing robustness and accuracy of advection schemes. The setup of the problem, initial conditions and description of the flow physics can be found in [23]. The problem has been studied intensively in recent years, see e.g. [3, 11] and references therein. The results of the conventional flux-expansion ADER schemes with the exact Riemann solver, HLL [6] and HLLC [19] Riemann solvers can be found in [15] for a sequence of meshes and are not shown here. Figs. 3–4 show numerical results of the new ADER3-GM scheme for three meshes: 240 × 60, 480 × 120 and 960 × 240. We see that the scheme produces the flow pattern generally accepted in the existing literature as correct. All discontinuities are well resolved and correctly positioned. The overall accuracy of our new ADER3-GM scheme compares well with that of the WENO scheme [11] and conventional state-expansion ADER schemes [15].

We remark that the resolution of delicate flow features, such as slip surfaces and the jet can be directly related to the accuracy of the Riemann solver used in the scheme. In particular, complete Riemann solvers with all waves in the Riemann problem solution, e.g. exact and HLLC Riemann solvers, give results superior to those of the incomplete ones, such as HLL and Rusanov solvers. Comparing our results with those reported in [11, 15], we observe that the accuracy of our new ADER-GM scheme is comparable with that of the ADER-HLLC scheme and superior to the ADER3-HLL and WENO schemes.

6 Concluding Remarks

In this paper we have presented a modification of the solution procedure for the derivative Riemann problem which does not require an approximate-state Riemann solver. Our new DRP solver extends very high order upwind schemes to a large class of hyperbolic systems of conservation laws for which the Riemann problem solution is not available. We implemented the new Derivative Riemann solver in the framework of finite-volume ADER schemes in multiple space dimensions and applied the new schemes to the compressible Euler equations of gas dynamics. The presented numerical results illustrate the very high order of accuracy as well as the essentially non-oscillatory property of the ADER schemes based on the new DRP solver.

Acknowledgments. Part of the paper was finalized during the stay of the second author at the Isaac Newton Institute for Mathematical Sciences, University of Cambridge and participation in the programme *Nonlinear Hyperbolic Waves in Phase Dynamics and Astrophysics*. The first author acknowledges the support provided by the Isaac Newton Institute for Mathematical Sciences, University of Cambridge, UK, as co-organizer of the six-month programme on *Nonlinear Hyperbolic Waves in Phase Dynamics and Astro-*

physics, January to July 2003, and the associated EPSRC senior visiting fellowship, grant No GR N09276.

References

[1] M. Ben-Artzi and J. Falcovitz. A second–order Godunov–type scheme for compressible fluid dynamics. *J. Comput. Phys.*, 55:1–32, 1984.

[2] J. Casper and H. Atkins. A finite-volume high order ENO scheme for two dimensional hyperbolic systems. *J. Comput. Phys.*, 106:62–76, 1993.

[3] B. Cockburn and C.-W. Shu. Runge-Kutta Discontinuous Galerkin methods for convection-dominated problems. *J. Sci. Comput.*, 16:173–261, 2001.

[4] M. Dumbser and C.-D. Munz. Building Blocks for Arbitrary High Order Discontinuous Galerkin Schemes. 2005. submitted to J. Sci. Comp.

[5] S.K. Godunov. A finite difference method for the computation of discontinuous solutions of the equations of fluid dynamics. *Mat. Sbornik*, 47:357–393, 1959.

[6] A. Harten, P. D. Lax, and B. van Leer. On upstream differencing and Godunov-type schemes for hyperbolic conservation laws. *SIAM Review*, 25(1):35–61, 1983.

[7] A. G. Kulikovskii, N. V. Pogorelov, and A. Yu. Semenov. *Mathematical Aspects of Numerical Solution of Hyperbolic Systems*. Chapman and Hall, 2002. Monographs and Surveys in Pure and Applied Mathematics, Vol. 118.

[8] I.S. Men'shov. Increasing the order of approximation of Godunov's scheme using the solution of the generalized Riemann problem. *U.S.S.R. Comput. Math. Math. Phys.*, 30(5):54–65, 1990.

[9] V.V. Rusanov. Calculation of interaction of non-steady shock waves with obstacles. *USSR J. Comp. Math. Phys.*, 1:267–279, 1961.

[10] T. Schwartzkopff, M. Dumbser, and C.D. Munz. Fast high order ADER schemes for linear hyperbolic equations. *J. Comput. Phys.*, 197(2):532–539, 2004.

[11] J. Shi, C. Hu, and C.-W. Shu. A technique for treating negative weights in WENO schemes. *J. Comput. Phys.*, 175:108–127, 2002.

[12] C.-W. Shu. Total - Variation - Diminishing time discretizations. *SIAM J. Scientific and Statistical Computing*, 9:1073–1084, 1988.

[13] Y. Takakura and E.F. Toro. Arbitrarily accurate non-oscillatory schemes for a nonlinear conservation law. *CFD Journal*, 11(1):7–18, 2002.

[14] V.A. Titarev and E.F. Toro. ADER: arbitrary high order Godunov approach. *J. Sci. Comput.*, 17:609–618, 2002.

[15] V.A. Titarev and E.F. Toro. ADER schemes for three-dimensional nonlinear hyperbolic systems. *J. Comput. Phys.*, 2005. in press.

[16] E.F. Toro. *Riemann Solvers and Numerical Methods for Fluid Dynamics.* Springer-Verlag, 1999. Second Edition.

[17] E.F. Toro. Riemann solvers with evolved initial conditions. *Preprint NI05003-NPA. Isaac Newton Institute for Mathematical Sciences, University of Cambridge, UK*, 2005.

[18] E.F. Toro, R.C. Millington, and L.A.M. Nejad. Towards very high order Godunov schemes. In E. F. Toro, editor, *Godunov Methods. Theory and Applications*, pages 907–940. Kluwer/Plenum Academic Publishers, 2001.

[19] E.F. Toro, M. Spruce, and W. Speares. Restoration of the Contact Surface in the Harten-Lax-van Leer Riemann Solver. *Journal of Shock Waves*, 4:25–34, 1994.

[20] E.F. Toro and V.A. Titarev. Solution of the generalised Riemann problem for advection-reaction equations. *Proc. Roy. Soc. London*, 458 (2018):271–281, 2002.

[21] E.F. Toro and V.A. Titarev. MUSTA schemes for systems of conservation laws. *Preprint NI04033-NPA. Isaac Newton Institute for Mathematical Sciences, University of Cambridge, UK*, 2004.

[22] E.F. Toro and V.A. Titarev. ADER schemes for scalar non-linear hyperbolic conservation laws with source terms in three-space dimensions. *J. Comput. Phys.*, 202(1):196–215, 2005.

[23] P. Woodward and P. Colella. The numerical simulation of two-dimensional fluid flow with strong shocks. *J. Comput. Phys.*, 54:115–173, 1984.